Journal of Inorganic and Organometallic Polymers and Materials (2021) 31:2161–2167
https://doi.org/10.1007/s10904-021-01929-y

Synthesis of $Ca_xCu_{3-x}Ti_4O_{12}$ Perovskite Materials and House-Hold LED Light Mediated Degradation of Rhodamine Blue Dye

Priyankamoni Saikia[1] · Hemanga Jyoti Sarmah[2] · Shahnaz Ahmed[1] · Suman Lahkar[1] · Jyoti Prakash Das[1] · Swapan Kumar Dolui[1]

Chapter 5

"Synthesis of $Ca_xCu_{3-x}Ti_4O_{12}$ Perovskite Materials and household LED light-mediated degradation of Rhodamine Blue dye"

Highlights: This chapter discusses the potential of oxide-based perovskite as photocatalyst. Synthesis of calcium copper titanate and its different compositions are mentioned and later, the exploration of their photocatalytic activities for the degradation of Rhodamine Blue dye using household blue LED light are demonstrated.

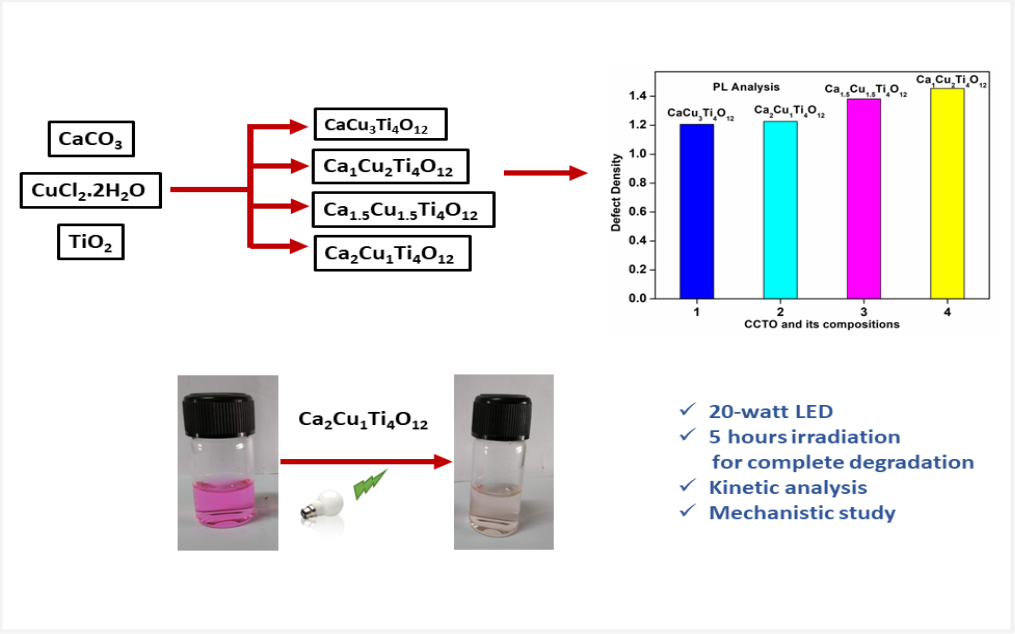

5.1 Introduction

In the 21st century, the rapid development of industrialization has immensely affected our ecosystem by discharging various pollutants and toxic components into our life cycle [1,2]. Among many life-threatening problems, one of the important areas to investigate is the treatment of toxic wastewater for the protection of human health and the ecosystem [3-5]. The dye degradation mainly possesses through various techniques such as chemical techniques (Ozonisation, Fenton-reagents etc.), physical techniques (Ion-exchange, Filtration etc.) and biological techniques (Aerobic degradation, biosorption etc.). Though various techniques are well-known and developed, the photocatalytic semiconductor-based oxidation process has emerged as one of the most probable techniques in sustainable chemistry. Photocatalyst plays a significant role in the degradation process. During the degradation process, the photocatalyst absorbs photons and generates excitons, electrons, and holes. These formed excitons help in the degradation of pollutants into some non-toxic components mostly H_2O and CO_2 [6-9]. Among various photocatalysts, TiO_2, CdS, ZnO, and WO_3 have been the most widely used photocatalytic materials in different conversion reactions [10-13]. Apart from many advantages, there have some noticeable disadvantages such as most of the materials have a larger bandgap and performed only through the UV light activation process. Our solar spectrum only possesses 5% UV light [14]. Moreover, the recombination energy of the materials is also high. Thus, the development of a photocatalyst with a narrow bandgap and high light absorbance capacity is highly beneficial.

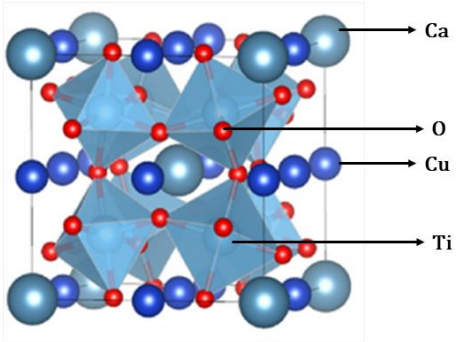

Figure 5.1 Crystal structure of perovskite CCTO

Nowadays, the perovskite-based photocatalyst has emerged as a new promising semiconductor material due to its unique photophysical and optoelectronic

properties [15-19]. The perovskite-based materials used for the photocatalytic purposes are $BaTiO_3$ [20], $CaTiO_3$ [21], $CoTiO_3$ [22], $NiTiO_3$ [23], $LaFeO_3$ [24], etc.

In the perovskite photocatalyst family, Calcium Copper Titanate (CCTO) is one of the early known perovskite compounds and its various applications have been witnessed due to its advantageous optical properties (Figure 5.1) [25-30]. The CCTO materials have been widely applied in the applications of capacitors, microwave devices, antennas, and sensors. The materials have a high dielectric constant [27]. During the solid-state synthetic route, solid precursor materials have been used to synthesize a well-defined structure. CCTO exhibits an outstanding dielectric permittivity (up to 10^4) [27]. Along with electronic properties, CCTO materials also exhibit excellent magnetic properties. The solid-state method has some disadvantages in maintaining purity as the synthesized materials contain some impurities such as $CaTiO_3$ and CuO etc [32,33]. The wet chemistry methods include polymerized complex [34,35], microwave dealing [36], and co-precipitation method [37], etc can be able to resolve the disadvantage of the solid-state method. To act as a photocatalyst, various works have been reported where CCTO was widely used as a photocatalyst while degrading many toxic dyes [38,39]. Zhu et al. studied the photocatalytic removal of ibuprofen drug using a CCTO photocatalyst under the illumination of visible light [39]. Similarly, Kushwaha et al. studied the photocatalytic degradation of Congo Red and Methyl Orange dyes using the composite CCTO-polyaniline in the illumination of a visible light source [17].

In the previous literature, though CCTO photocatalysts were well-recognized in dye-degradation although the proper correlation of the defect density with the photocatalytic degradation of the specimen and CCTO hasn't been addressed. In this chapter, we demonstrated the synthesis of the CCTO-derived materials ($Ca_xCu_{3-x}Ti_4O_{12}$, where x = 1, 1.5, 2) by citrate precursor method by changing the molar ratios of Ca^{2+} and Cu^{2+} and studied their photoluminescence (PL) properties. The photocatalytic behaviour of the CCTO perovskite with respect to Rhodamine Blue dye was investigated by varying the composition ($Ca_xCu_{3-x}Ti_4O_{12}$, where x=1,1.5,2) Additionally, a comparative study of degradation efficiency and rate constant with the defect concentration is established.

5.2 Experimental

5.2.1 Materials

Calcium carbonate, $CaCO_3$ (98.5%, Avantor), copper chloride dihydrate, $CuCl_2.2H_2O$ (99.0%, Merck), anhydrous citric acid, $C_6H_8O_7$ (99.0%, Merck), titanium dioxide, TiO_2 (98.5%, Merck), Rhodamine Blue (RhB) (99.9 %, Alfa Aesar) were purchased from standard source and used as starting material, without any further purification.

5.2.2 Synthesis of Calcium Copper Titanate ($Ca_xCu_{3-x}Ti_4O_{12}$) and its compositions

The perovskite, Calcium Copper Titanate (CCTO), and its compositions were synthesized by a conventional citrate precursor method as reported by Turky and co-workers [40]. To synthesize CCTO ($CaCu_3Ti_4O_{12}$), the aqueous solution of $CaCO_3$, $CuCl_2.2H_2O$, and TiO_2 were mixed in a molar ratio of 1:3:4 respectively. Citric Acid is added as a complexing agent in the ratio 1:5 of metal precursor to the citric acid. The obtained light-coloured solution was slowly heated at 80 ℃ to form a gel. Subsequently, the gel was calcinated at 1000 ℃ for 2 hours at a heating rate of 10 ℃/min in a muffle furnace to achieve the target material $CaCu_3Ti_4O_{12}$ in the perovskite structure. To prepare the CCTO-derived material in various compositions, the above-mentioned compounds are now mixed in the different ratios of Ca_x:Cu_{3-x}: Ti_4:O_{12} where x = 1, 1.5, and 2 [40]. The synthesized materials are named CCTO (x = 1), CCTO (x = 1.5), and CCTO (x = 2), respectively.

5.2.3 Characterization

To confirm the structure analysis, X-ray Diffraction (XRD) studies were carried out using a Rigaku Miniflex X-ray diffractometer (Tokyo, Japan), equipped with CuK_α radiation (λ = 0.15418 nm, scanning rate = 0.05 s^{-1}) at 30 kV and 15 mA, where data is acquired in the 2θ range of 7° to 80°. In addition, FT-IR spectra of the samples were recorded with a Nicolet Impact-410 IR spectrometer (USA) in the KBr medium at room temperature in the range of 4000–400 cm^{-1}, to have a proper understanding of IR active bonds present in the host system. In optical studies, absorption and emission spectra were acquired using a Shimadzu UV-2550 and Hitachi F-2700 fluorescence spectrophotometer respectively. For morphological and elemental analysis, a Scanning electron Microscope (SEM) and energy dispersive X-ray analysis technique (JEOL-JSM-6390LV) were employed.

5.2.4. Photodegradation procedure

Light emitting diodes (LEDs) presents various advantages of optical properties, including low consumption energy, long-lasting life, narrow-spectrum luminescence properties, etc. In this chapter, available and domestic used visible LED light of 20 W (Philips LED lamp B22, 2000 lumen) was used as a light source to excite the excitons. The bulb was placed at 8 cm apart from the reaction vessel (top of it). The whole photocatalytic reaction vessel was encircled by a cardboard box of dimensions 44×35×36.5 cm^3 (length×width×height). The reaction was carried out at a room temperature of 30 ± 5 ^oC. The target dye {i.e., Rhodamine Blue (RhB)} stock solution considered for the study at a concentration of 100 ppm in distilled water was prepared. Photodegradation of RhB dye solution was carried out in a Shimadzu UV-2550 spectrophotometer using a path length of ~1 cm. For the photocatalytic experiment, 50 mg of catalyst was added to a 5 mL (100 ppm) dye stock solution which was diluted by 95 mL H_2O and 1 mL H_2O_2 and stirred in dark for 12 hours to attain the adsorption/desorption equilibrium. LED was switched on to start the photocatalytic experiment, which was continued for several hours. At a certain interval, 5 mL of the aliquot was taken out from the reactor and centrifuged it and the dye content in the solution was analysed through absorption spectroscopy.

5.3 Results and Discussion

5.3.1 Structural Analysis

5.3.1.1 XRD spectra

The XRD technique was recorded to analyse the phases of the synthesized CCTO and its compositions (x = 1, 1.5, 2). From the spectra (Figure 5.2), it is confirmed that the diffraction planes (220), (400), and (422) are corresponding to the cubic phase of CCTO in accordance with JCPDS No. 75-2188 [40]. Due to the presence of impurities like CuO and TiO_2, some secondary weak diffraction peaks were also observed [40].

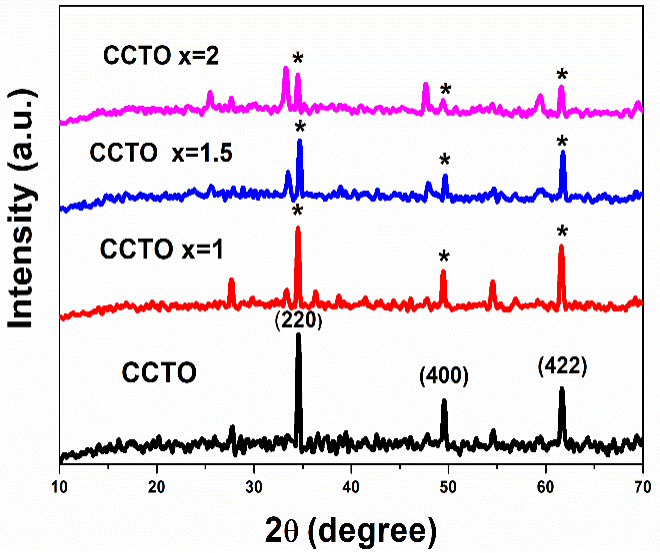

Figure 5.2 XRD pattern of CCTO and its compositions (x = 1, 1.5, 2)

The lattice parameter and the unit cell volume for the perovskites and their compositions were calculated by using following equations [41]:

$$d_{hkl} = \frac{a}{\sqrt{h^2+k^2+l^2}}$$

$$V_{cell} = a^3$$

The degree of crystallinity was calculated with the help of following equation [42]:

$$Crystallinity = \frac{Area\ of\ crystallite\ peak}{\text{Area of all peaks}}$$

In addition, the average crystallite size was calculated by Debye-Scherrer formula [43]:

$$D = \frac{0.9\lambda}{B\cos\theta}$$

In the above equation, D and λ are defined as the crystallite size and the wavelength of CuK_α radiation, and 2θ and B are defined as peak position and the full-width half maximum (FWHM) in radians respectively. The variations in structural parameters are outlined in the Table 5.1.

Table 5.1 Structural parameters of prepared CCTO and compositions (x = 1, 1.5, 2)

Entry	CCTO Compositions	Volume of the unit cell (cm^{-3})	Crystallinity (%)	Crystallite size (nm)
1	CCTO	0.433333	8.48	22.0
2	CCTO (x=1)	0.396133	10.6	21.1
3	CCTO (x=1.5)	0.394767	8.51	16.7
4	CCTO (x=2)	0.40135	8.48	16.1

5.3.1.2 FT-IR spectra

To obtain further information on the materials, FT-IR spectra of CCTO and its compositions (x = 1, 1.5, 2) were recorded (Figure 5.3). The broad absorption peak at ~3430 cm^{-1} is attributed due to the O-H stretching frequency of the adsorbed moisture [44]. The absorption peak at ~463 cm^{-1} is due to the Ti-O-Ti stretching frequency [45]. In addition, the bending vibration of Cu-O and Ca-O appears at ~525 cm^{-1} at 606 cm^{-1}, respectively [45]. The absorption peak is located at 380-700 cm^{-1} corresponds to the mixed vibrations of TiO_6 and CuO_4 [45]. Also, as the compositions of the copper content were reduced gradually in the CCTO materials during the synthesis, as a result, the peak intensity corresponding to Cu-O (~525 cm^{-1}) got gradually decreased.

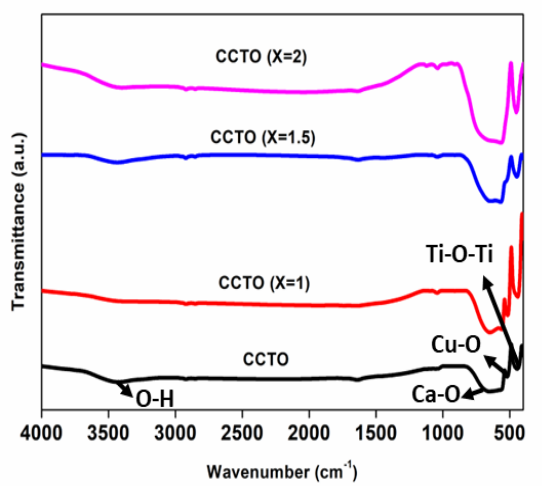

Figure 5.3 FT-IR spectra of CCTO and its compositions (x = 1, 1.5, 2)

5.3.1.3 Morphological Analysis (SEM analysis)

The SEM analysis and resultant image of the perovskite CCTO revealed the structural feature of the compound (Figure 5.4) which shows a cubic-shaped polyhedral

structure. The figure in this study depicted the presence of large microstructure matrix, where small grains were ingrained in between the large grains. The polyhedral shape structured photocatalysts provide a better candidate to pursue their catalytic activities [19, 46]. The calculated average particle size of the synthesized materials were found to be 1µm.

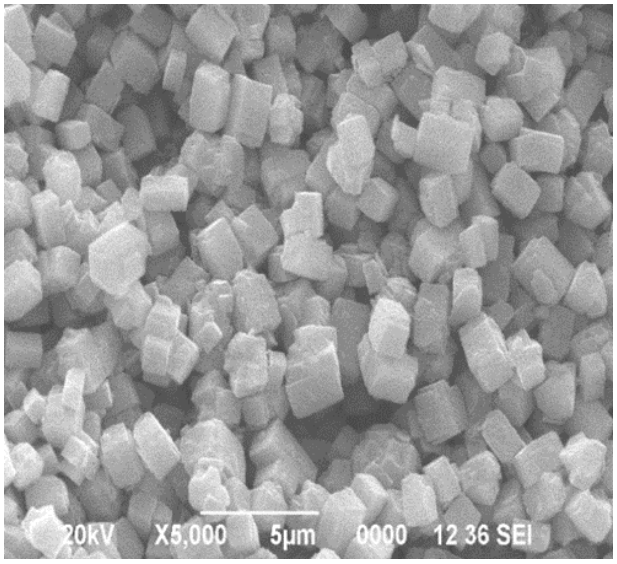

Figure 5.4 SEM image of CCTO composition

5.3.1.4 Energy Dispersive X-ray spectrum (EDX analysis)

EDX spectra of the synthesized materials revealed the presence of Ca, Cu, Ti, and O elements in the host material with a close approximation elemental ratio to their atomic percentages (Figure 5.5).

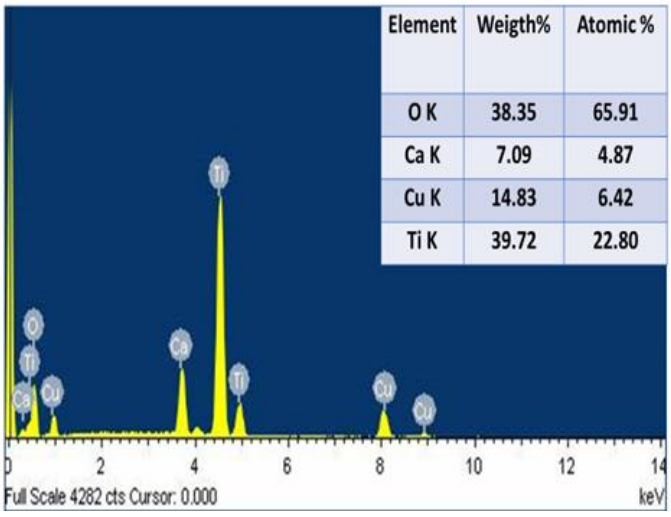

Figure 5.5 EDX spectra of CCTO

5.3.2 Optical analysis

The absorption properties were studied through UV-Vis spectra in the range of 200 to 800 nm. The band gap energy was calculated using the Tauc plot method from the absorption spectra in accordance with the following relation [40]:

$$(\alpha h\nu)^m = h\nu - Eg$$

In the above equation, α is the optical absorption coefficient, h is Planck's constant, ν is the Photon's frequency, Eg is the bandgap energy [40] and m is a constant associated with the type of transitions (m = 1/2 to indirect transitions and m = 2 for direct transitions) [47]. In this case, the optical transitions, that are allowed to direct band-to-band transition was considered . The calculated band gaps for CCTO, CCTO (x = 1), CCTO (x = 1.5), and CCTO (x = 2) were found as 2.18, 1.93, 2.40, and 2.55 eV, respectively (Figure 5.6 b). Moreover, it was assumed that the incorporation of Ca or Cu in the CCTO lattice causes some distortions between TiO_6 and CaO leading to the appearance of some intermediate levels (defect states) might appear in between the valence band and conduction band [40,48].

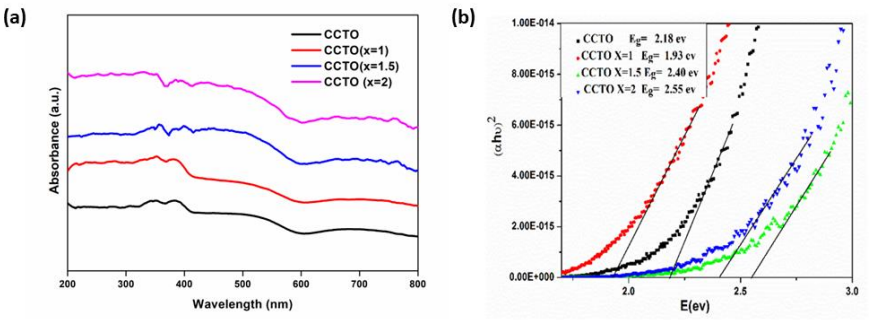

Figure 5.6 (a) Absorption plots for all CCTO (b) Optical band gap calculations of CCTO and its compositions (x = 1, 1.5, 2) using the Tauc plot method

Later, the luminescence properties of CCTO and its compositions (x = 1, 1.5, 2) were studied through photoluminescence spectroscopy (Figure 5.7 and Figure 5.8). The excitation peak for the luminescent spectra was fixed in accordance with the highest absorbance intensity of the respective absorbance spectra. Hence, an asymmetrical and broad emission spectrum was observed implying the presence of surface or defect states in the host system [49]. Upon deconvolution, multiple peaks for a band gap excitations were observed. The first peak appearing near the band gap may be

assigned for the near band edge emission. At the same time, other peaks could be associated with the defective origin, which usually appears in the forbidden regions . The defect density of the system was estimated by measuring the integral intensity (area under the curve) of the second peak, compared to the near band-edge emission (NBE) peak. Theoretically, the integral intensity for a defective peak qualitatively represents better defect concentration in the system. The large integral intensity of defective peak with respect to NBE for CCTO (x = 1) compared to the other samples, implying the highest defect concentration which might lead to better photocatalytic activity (Table 5.2).

Table 5.2 Comparison of defect density of different compositions of the photocatalyst

Photocatalyst	Integral intensity of the defective peak
CCTO	1.2086
CCTO (x = 1)	1.454
CCTO (x = 1.5)	1.382
CCTO (x = 2)	1.227

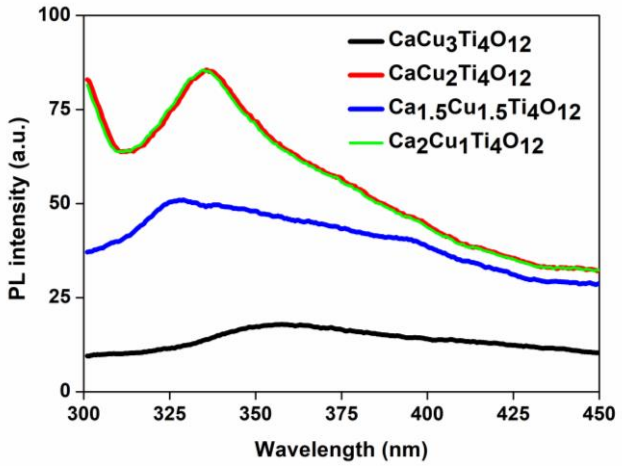

Figure 5.7 Photoluminescence emission spectra of CCTO and its compositions (x = 1, 1.5, 2)

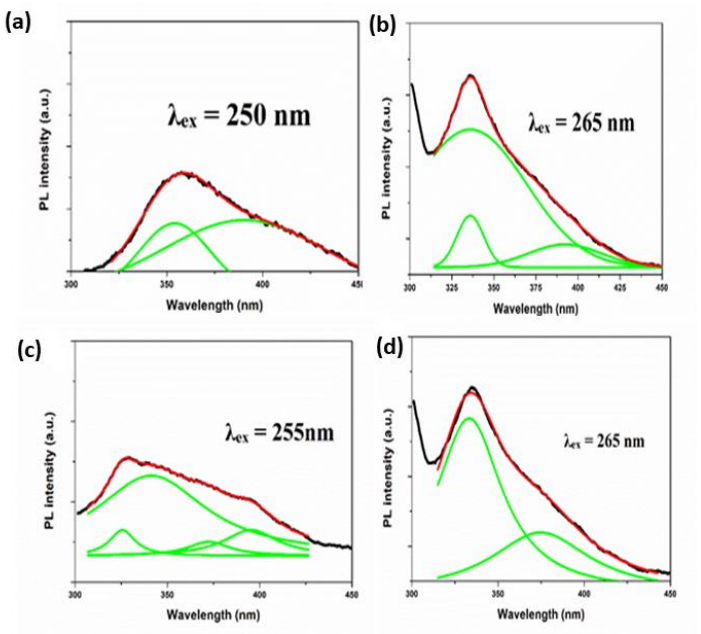

Figure 5.8 (a) PL emission spectra of CCTO, (b) PL emission spectra of CCTO (x = 1), (c) PL emission spectra of CCTO (x = 1.5), and (d) PL emission spectra of CCTO (x = 2) (The color code green signifies the deconvoluted peaks and red signifies the red color signifies the merged peaks of the deconvoluted peaks)

5.3.3 Photocatalytic activity

To study the photocatalytic behaviour of the materials, the study selected a domestic household 20-Watt LED bulb as a light source, and Rhodamine dye (RhB) as a standard pollutant. The degradation of the RhB stock solution was studied with respect to the highest absorption peak at 552 nm. The prepared catalyst was added to the dye-stock solution and stirred for a period of 12 h to achieve adsorption-desorption equilibrium. Upon exposure to the LED light, the absorption spectra of the RhB gradually decrease which signifies the degradation process (Figure 5.9). After illumination for a period of 6 h, the degradation percentage of RhB was calculated by using the following equation [50]:

$$Degradation\ rate\ (r) = \frac{C_0 - C}{C_0} \times 100\%$$

The calculated degradation efficiency values for CCTO, CCTO (x = 1), CCTO (x = 1.5), and CCTO (x = 2) were found as 62.5%, 99.42%, 37.17%, and 47.28%, respectively. From the observed values, it was found that the prepared catalyst CCTO (x = 1) exhibited better photocatalytic performance. In this equation, C_0 and C are the concentration of Rhodamine Blue solution at t=0 (initial), and any time t, respectively

[50]. As the absoprtion in UV-Vis spectra depends on the concentration, so the above equation can be written in terms of absorbance, A_o (initial) and A (any time t):

$$r \quad = \frac{A_o - \mathrm{A}}{A_o} \times 100\%$$

Furthermore, the kinetics of photocatalytic degradation of Rhodamine Blue was investigated by plotting the degradation data in the integrated rate law expression for the 1st-order kinetics.

$$\ln (C_o/C) = kt + \text{constant}$$

In the above equation, k is the first-order rate constant (unit is min^{-1}), which can be calculated from the slope of the graph of ln (C_o/C) versus irradiate time t [38, 50, 51].

The rate constant for CCTO (x = 1) was found 1.93×10^{-2} min^{-1} and it was higher than that of the other three compositions. This result can be attributed due to the higher defect density than that of the other compositions and in addition, it may be ensured from the luminescence studies (Figure 5.10). The comparison graph showed the increment of defect density initially with varying x-value before achieving saturation (Figure 5.11). When the material was changed from CCTO to its composition (x = 1), the defect density was found to improve, resulting in an enhancement of the reaction rate. Analysing the same for compositions x = 1.5 and 2, the defect density was observed declination gradually. The rate constant was dropped in a similar trend abruptly (with x = 1.5), before getting saturated. The comparison of the degradation efficiency and rate constants for different catalyst were shown in the Table 5.3. In our study, the best result was observed for (x = 1) compositions, favouring a better degradation rate constant.

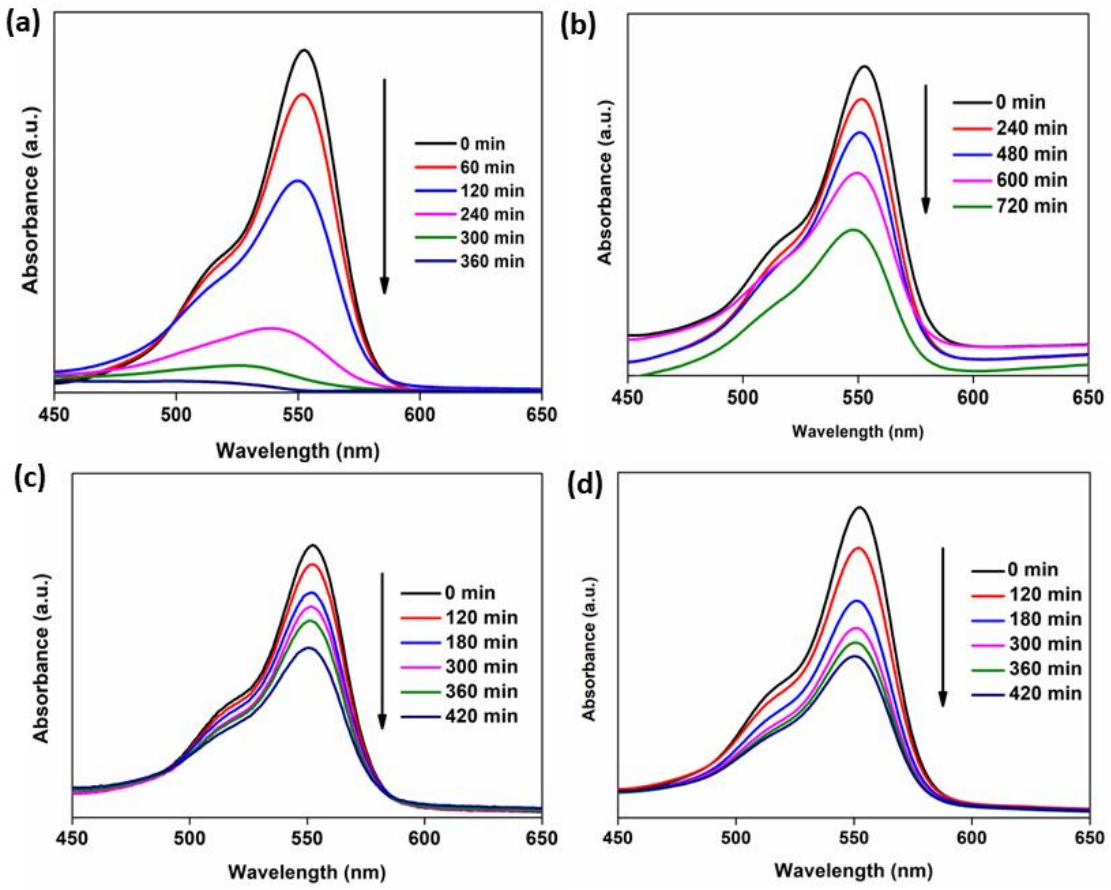

Figure 5.9 Time-dependent UV-Vis spectrum changes of Rhodamine blue (100 ppm) solution catalysed by (a) CCTO (x = 1), (b) CCTO, (c) CCTO (x = 1.5) and (d) CCTO (x = 2) respectively

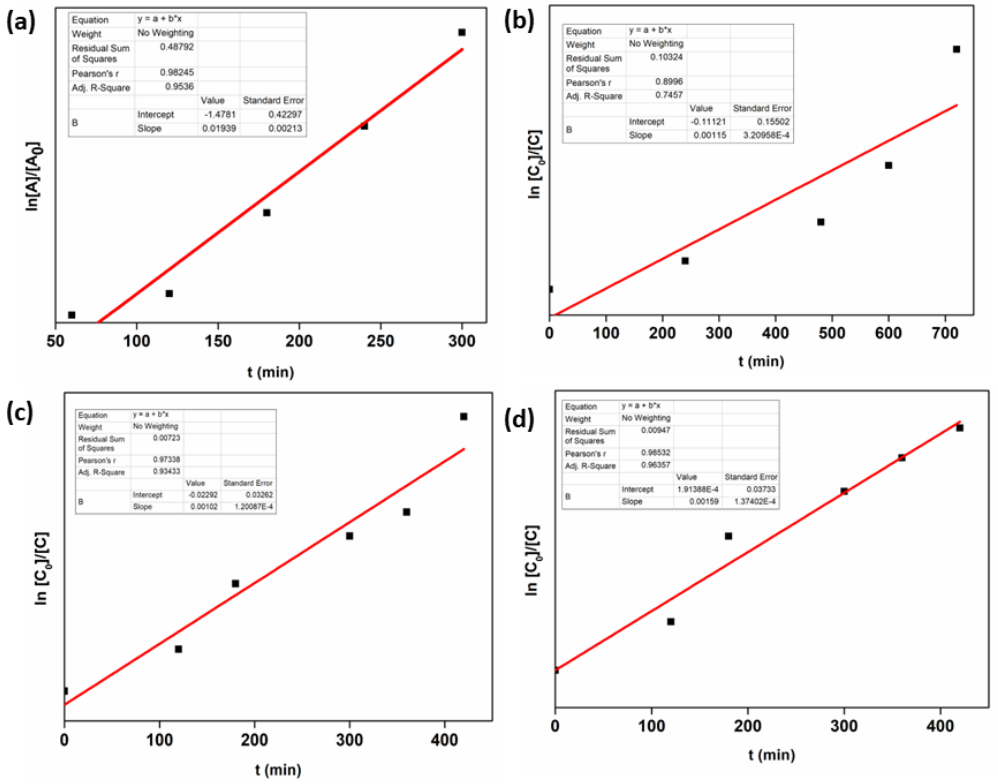

Figure 5.10 ln [C_0]/[C] versus time plot by (a) CCTO (x = 1), (b) CCTO, (c) CCTO (x = 1.5), and (d) CCTO (x = 2) respectively

The composition CCTO (x = 1) showed the most satisfactory result by degrading 99.42% in only 6 h. On the other hand, the other composite CCTO (x = 1.5) and CCTO (x = 2) exhibited only 37.17% and 47.28% degradation within 420 min.

Table 5.3 Comparison of degradation efficiency of different compositions of the photocatalyst

Photocatalyst	Degradation percentage (%)	Irradiation time (min)	Degradation rate constant (min^{-1})
CCTO	62.5	720	0.11×10^{-2}
CCTO (x = 1)	99.42	360	1.93×10^{-2}
CCTO (x = 1.5)	37.17	420	0.10×10^{-2}
CCTO (x = 2)	47.28	420	0.15×10^{-2}

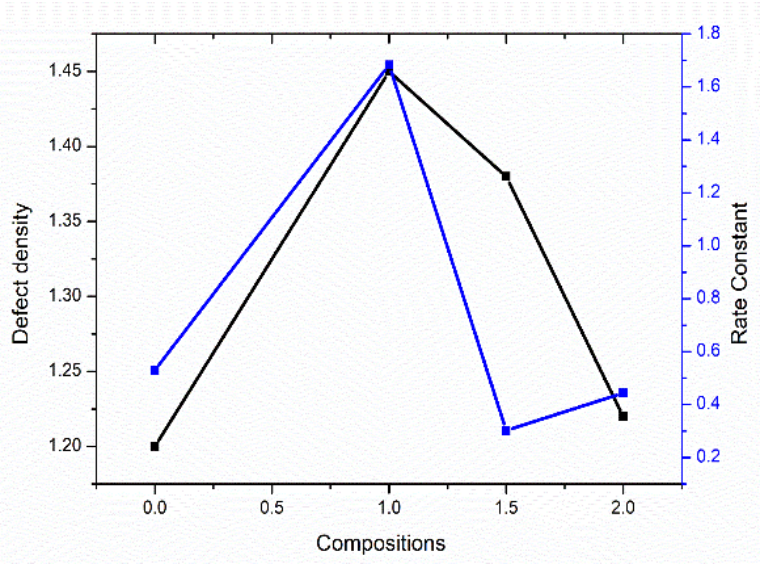

Figure 5.11 Variation of rate constant and defect density, with x-value

5.3.4 Mechanistic insight

To determine the active species in the degradation of Rhodamine Blue, various scavenger test was performed in further study. Isopropanol is a well-known OH· scavenger and *p*-benzoquinone is a $O_2^{\cdot-}$ radical scavenger. The degradation of RhB in the presence of various scavengers was highlighted in Figure 5.12. In addition to benzoquinone (BQ), the degradation process showed suppression, which indicates that the main active species in the degradation process is superoxide anion ($O_2^{\cdot-}$). This study unequivocally supports photocatalytic degradation. The mechanism of the process was proposed from these initial studies. When the visible light is irradiated on the surface of the CCTO catalyst, electrons, and holes form in the valence and conduction bands (Figure 5.13). The number of holes generated in the valence band is the same as the number of electrons generated in the conduction band [51]. The electrons (from the conduction band) then react with absorbed oxygen to generate reactive superoxide ($O_2^{\cdot-}$) radical which further reacts with water to produce hydroxyl radical (OH·). On the other hand, holes (in the valence band) react with a water molecule and generate OH· radical [50].

The stepwise reactions are given below:

$$CCTO + h\nu = CCTO(h^+ + e^-)$$

$$CCTO(h^+) + H_2O = H^+ + OH^-$$

$$CCTO(e^-) + O_2(\text{absorbed}) = CCTO + {O_2}^{-\cdot}$$

$$CCTO(e^-) + H_2O_2 = CCTO + OH^{\cdot} + OH^-$$

$$O_2^{-\cdot} + H_2O = OH^{\cdot}$$

$$OH^{\cdot} + \text{Rhodamine Blue (dye)} = H_2O + CO_2 + NO_3^{-}$$

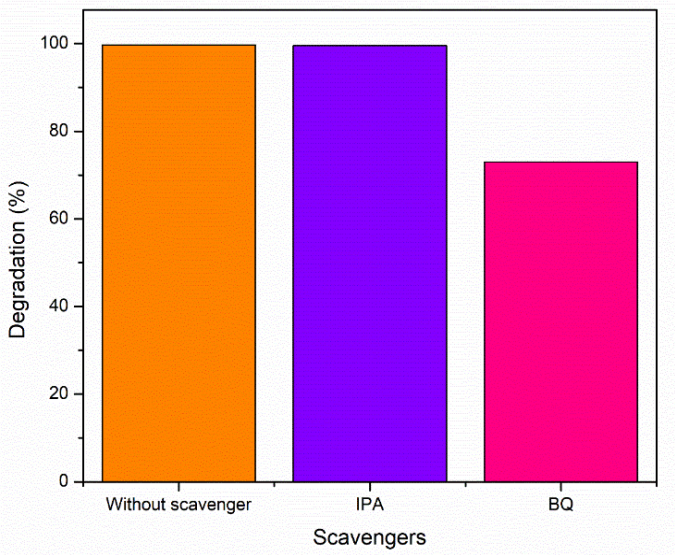

Figure 5.12 Photocatalytic degradation of Rhodamine blue in the presence of various scavengers

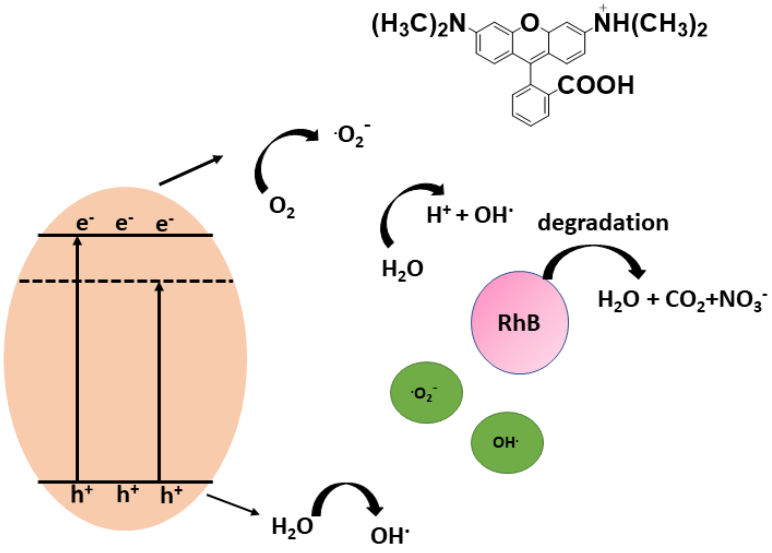

Figure 5.13 Plausible mechanism degradation of RhB dye under LED with CCTO

5.4 Conclusion

In conclusion, this chapter discussed the preparation of perovskite photocatalyst calcium copper titanate (CCTO) and its compositions *via* the citrate precursor

method. The photocatalytic property of the material was examined through the degradation of Rhodamine Blue dye under the illumination of 20-Watt LED light. The efficiency of the degradation for the composition CCTO (x = 1) was higher, having a degradation efficiency of 99.42% within 6 hours. Furthermore, the kinetic studies of the degradation process reveal 1st order kinetics with the composition x = 1 showed the higher rate constant of the reaction in comparison to other compositions. The PL study of the materials justified the higher defect concentration and followed by its photocatalytic performance. This simple 20-watt LED light driven protocol for photodegradation of dye could be very useful for medium scale pollutant cleaning or might be possible in practical application.

5.5 Bibliography

[1] Lellis, B., Fávaro-Polonio, C. Z., Pamphile, J. A., and Polonio, J. C. Effects of textile dyes on health and the environment and bioremediation potential of living organisms. *Biotechnology Research and Innovation*, 3(2):275-290, 2019.

[2] Yaseen, D. and Scholz, M. Textile dye wastewater characteristics and constituents of synthetic effluents: a critical review. *International Journal of Environmental Science and Technology*, 16:1193-1226, 2019.

[3] Mitra, M., Ahamed, S. T., Ghosh, A., Mondal, A., Kargupta, K., Ganguly, S., and Banerjee, D. Polyaniline/reduced graphene oxide composite-enhanced visible-light-driven photocatalytic activity for the degradation of organic dyes. *ACS Omega*, 4(1):1623-1635, 2019.

[4] Kulsi, C., Ghosh, A., Mondal, A., Kargupta, K., Ganguly, S., and Banerjee, D. Remarkable photo-catalytic degradation of malachite green by nickel doped bismuth selenide under visible light irradiation. *Applied Surface Science*, 392:540-548, 2017.

[5] Sarkar, C., Bora, C., and Dolui, S. K. Selective dye adsorption by pH modulation on amine-functionalized reduced graphene oxide–carbon nanotube hybrid. *Industrial & Engineering Chemistry Research*, 53(42):16148-16155, 2014.

[6] Ghosh, A., Mitra, M., Banerjee, D., and Mondal, A. Facile electrochemical deposition of Cu_7Te_4 thin films with visible light driven photocatalytic activity and thermoelectric performance. *RSC Advances*, 6(27):22803-22811, 2016.

[7] Li, X., Xie, J., Jiang, C., Yu, J., and Zhang, P. Review on design and evaluation of environmental photocatalysts. *Frontiers of Environmental Science & Engineering*, 12:1-32, 2018.

[8] Dong, S., Feng, J., Fan, M., Pi, Y., Hu, L., Han, X., Liu, M., Sun, J., and Sun, J. Recent developments in heterogeneous photocatalytic water treatment using visible light-responsive photocatalysts: a review. *RSC Advances*, 5(19):14610-14630, 2015.

[9] Opoku, F., Govender, K. K., van Sittert, C. G. C. E. and Govender, P. P. Recent progress in the development of semiconductor-based photocatalyst materials for applications in photocatalytic water splitting and degradation of pollutants. *Advanced Sustainable Systems*, 1(7):1700006, 2017.

[10] Yang, J., Chen, C., Ji, H., Ma, W., and Zhao, J. Mechanism of TiO_2-assisted photocatalytic degradation of dyes under visible irradiation: photoelectrocatalytic study by TiO_2-film electrodes. *The Journal of Physical Chemistry B*, 109(46):21900-21907, 2005.

[11] Sher Shah, M. S. A., Park, A. R., Zhang, K., Park, J. H., and Yoo, P. J. Green synthesis of biphasic TiO_2–reduced graphene oxide nanocomposites with highly enhanced photocatalytic activity. *ACS Applied Materials & Interfaces*, 4(8):3893-3901, 2012.

[12] Intarasuwan, K., Amornpitoksuk, P., Suwanboon, S., and Graidist, P. Photocatalytic dye degradation by ZnO nanoparticles prepared from $X_2C_2O_4$ (X = H, Na and NH_4) and the cytotoxicity of the treated dye solutions. *Separation and Purification Technology*, 177:304-312, 2017.

[13] Liu, X., Zhai, H., Wang, P., Zhang, Q., Wang, Z., Liu, Y., Dai, Y., Huang, B., Qin, X., and Zhang, X. Synthesis of a WO_3 photocatalyst with high photocatalytic activity and stability using synergetic internal Fe^{3+} doping and superficial Pt loading for ethylene degradation under visible-light irradiation. *Catalysis Science & Technology*, 9(3):652-658, 2019.

[14] Magalhaes, P., Andrade, L., Nunes, O. C., and Mendes, A. Titanium dioxide photocatalysis: Fundamentals and application on photoinactivation. *Reviews on Advanced Materials Science*, 51(2), 2017.

[15] Clark, J. H., Dyer, M. S., Palgrave, R. G., Ireland, C. P., Darwent, J. R., Claridge, J. B., and Rosseinsky, M. J. Visible light photo-oxidation of model pollutants

using $CaCu_3Ti_4O_{12}$: an experimental and theoretical study of optical properties, electronic structure, and selectivity. *Journal of The American Chemical Society*, 133(4):1016-1032, 2011.

[16] Sen, A. and Chattopadhyay, K. K. Nanostructured $CaCu_3Ti_4O_{12}$ for environmental remediation through visible light active catalysis. *Journal of Materials Science: Materials in Electronics*, 27:10393-10398, 2016.

[17] Kushwaha, H., Thomas, P., and Vaish, R. Polyaniline/$CaCu_3Ti_4O_{12}$ nanofiber composite with a synergistic effect on visible light photocatalysis. *RSC Advances*, 5(106):87241-87250, 2015.

[18] Otitoju, T. A., Jiang, D., Ouyang, Y., Elamin, M. A. M., and Li, S. Photocatalytic degradation of Rhodamine B using $CaCu_3Ti_4O_{12}$ embedded polyethersulfone hollow fiber membrane. *Journal of Industrial and Engineering Chemistry*, 83:145-152, 2020.

[19] Kanhere, P. and Chen, Z. A review on visible light active perovskite-based photocatalysts. *Molecules*, 19(12):19995-20022, 2014.

[20] Maeda, K. Rhodium-doped barium titanate perovskite as a stable p-type semiconductor photocatalyst for hydrogen evolution under visible light. *ACS Applied Materials & Interfaces*, 6(3):2167-2173, 2014.

[21] Zhang, H., Chen, G., Li, Y., and Teng, Y. Electronic structure and photocatalytic properties of copper-doped $CaTiO_3$. *International Journal of Hydrogen Energy*, 35(7):2713-2716, 2010.

[22] Qu, Y., Zhou, W., and Fu, H. Porous cobalt titanate nanorod: a new candidate for visible light-driven photocatalytic water oxidation. *ChemCatChem*, 6(1):265-270, 2014.

[23] Qu, Y., Zhou, W., Ren, Z., Du, S., Meng, X., Tian, G., Pan, K., Wang, G., and Fu, H. Facile preparation of porous $NiTiO_3$ nanorods with enhanced visible-light-driven photocatalytic performance. *Journal of Materials Chemistry*, 22(32):16471-16476, 2012.

[24] Tijare, S. N., Joshi, M. V., Padole, P. S., Mangrulkar, P. A., Rayalu, S. S., and Labhsetwar, N. K. Photocatalytic hydrogen generation through water splitting on nano-crystalline $LaFeO_3$ perovskite. *International Journal of Hydrogen Energy*, 37(13):10451-10456, 2012.

[25] Ahmadipour, M., Arjmand, M., Abd Aziz, S. N. Q. A., Chiam, S. L., Ahmad, Z. A., and Pung, S. Y. Influence of annealing temperature on morphological and photocatalytic activity of sputter-coated $CaCu_3Ti_4O_{12}$ thin film under ultraviolet light irradiation. *Ceramics International*, 45(16):20697-20703, 2019.

[26] Hailili, R., Wang, Z. Q., Gong, X. Q., and Wang, C. Octahedral-shaped perovskite $CaCu_3Ti_4O_{12}$ with dual defects and coexposed {(001),(111)} facets for visible-light photocatalysis. *Applied Catalysis B: Environmental*, 254:86-97, 2019.

[27] Kawrani, S., Boulos, M., Cornu, D., and Bechelany, M. From synthesis to applications: copper calcium titanate (CCTO) and its magnetic and photocatalytic properties. *ChemistryOpen*, 8(7):922-950, 2019.

[28] Sinclair, D. C., Adams, T. B., Morrison, F. D., and West, A. R. $CaCu_3Ti_4O_{12}$: One-step internal barrier layer capacitor. *Applied Physics Letters*, 80(12):2153-2155, 2002.

[29] Pal, K., Dey, A., Ray, P. P., Mordvinova, N. E., Lebedev, O. I., Mandal, T. K., Seikh, M. M., and Gayen, A. Synthesis, Characterization and Catalytic Activity of Quadruple Perovskite: $CaCu_{3-x}Mn_xTi_{4-x}Mn_xO_{12}$ (x = 0, 0.5 and 1.0). *ChemistrySelect*, 3(4):1076-1087, 2018.

[30] Pansara, P., Meshiya, U., Makadiya, A., Raval, P., Modi, K., and Nambissan, P. Defect structure transformation during substitution in quadruple perovskite $CaCu_{3-x}Ti_{4-x}Fe_{2x}O_{12}$ studied by positron annihilation spectroscopy. *Ceramics International*, 45(15):18599-18603, 2019.

[31] Moura, F., Cabral, A., Rocha, L., Aguiar, E., Simões, A., and Longo, E. Photoluminescence emission in zirconium-doped calcium copper titanate powders. *Ceramics International*, 42(4):4837-4844, 2016.

[32] Thongbai, P., Yamwong, T., Maensiri, S., Amornkitbamrung, V., and Chindaprasirt, P. Improved dielectric and nonlinear electrical properties of fine-grained $CaCu_3Ti_4O_{12}$ ceramics prepared by a glycine-nitrate process. *Journal of the American Ceramic Society*, 97(6):1785-1790, 2014.

[33] Thongbai, P., Yamwong, T., Maensiri, S., Amornkitbamrung, V., and Chindaprasirt, P. Improved dielectric and nonlinear electrical properties of fine-grained $CaCu_3Ti_4O_{12}$ ceramics prepared by a glycine-nitrate process. *Journal of the American Ceramic Society*, 97(6):1785-1790, 2014.

[34] Rai, A. K., Singh, N. K., Lee, S. K., Mandal, K., Kumar, D., and Parkash, O. Dielectric properties of iron doped calcium copper titanate, $CaCu_{2.9}Fe_{0.1}Ti_4O_{12}$. *Journal of Alloys and Compounds*, 509(36):8901-8906, 2011.

[35] Jesurani, S., Kanagesan, S., Kalaivani, T., and Ashok, K. Dielectric properties of Erbium doped $CaCu_3Ti_4O_{12}$ prepared by sol–gel self-combustion method. *Journal of Materials Science: Materials in Electronics*, 23:692-696, 2012.

[36] Liu, J., Sui, Y., Duan, C. G., Mei, W. N., Smith, R. W., and Hardy, J. R. $CaCu_3Ti_4O_{12}$: Low-temperature synthesis by pyrolysis of an organic solution. *Chemistry of Materials*, 18(16):3878-3882, 2006.

[37] Xu, D., He, K., Yu, R., Sun, X., Yang, Y., Xu, H., Yuan, H., and Ma, J. High dielectric permittivity and low dielectric loss in sol–gel derived Zn doped $CaCu_3Ti_4O_{12}$ thin films. *Materials Chemistry and Physics*, 153:229-235, 2015.

[38] Pal, K., Mondal, A., Jana, R., Ray, P. P., and Gayen, A. Domestic LED light driven methylene blue degradation by g-C_3N_4-$CaCu_3Ti_4O_{12}$ composite. *Applied Surface Science*, 467:543-553, 2019.

[39] Zhu, Y., Wang, T., Wang, W., Chen, S., Lichtfouse, E., Cheng, C., Zhao, J., Li, Y., and Wang, C. $CaCu_3Ti_4O_{12}$, an efficient catalyst for ibuprofen removal by activation of peroxymonosulfate under visible-light irradiation. *Environmental Chemistry Letters*, 17:481-486, 2019.

[40] Turky, A. O., Rashad, M. M., Zaki, Z. I., Ibrahim, I. A., and Bechelany, M. Tuning the optical and dielectric properties of calcium copper titanate $Ca_xCu_{3-x}Ti_4O_{12}$ nanopowders. *RSC Advances*, 5(24):18767-18772, 2015.

[41] Liu, J., Smith, R. W., and Mei, W. N. Synthesis of the giant dielectric constant material $CaCu_3Ti_4O_{12}$ by wet-chemistry methods. *Chemistry of Materials*, 19(24):6020-6024, 2007.

[42] Lopez-Rubio, A., Flanagan, B. M., Gilbert, E. P., and Gidley, M. J. A novel approach for calculating starch crystallinity and its correlation with double helix content: A combined XRD and NMR study. *Biopolymers: Original Research on Biomolecules*, 89(9):761-768, 2008.

[43] Zak, A. K., Majid, W. A., Abrishami, M. E., and Yousefi, R. X-ray analysis of ZnO nanoparticles by Williamson–Hall and size–strain plot methods. *Solid State Sciences*, 13(1):251-256, 2011.

[44] Yang, J., Tang, Z., Yin, H., Liu, Y., Wang, L., Tang, H., and Li, Y. Poly (arylene ether nitrile) composites with surface-hydroxylated calcium copper titanate particles for high-temperature-resistant dielectric applications. *Polymers*, 11(5):766, 2019.

[45] Jesurani, S., Kanagesan, S., Velmurugan, R., and Kalaivani, T. Phase formation and high dielectric constant of calcium copper titanate using sol–gel route. *Journal of Materials Science: Materials in Electronics*, 23:668-674, 2012.

[46] Mogyorósi, K., Balázs, N., Srankó, D., Tombácz, E., Dékány, I., Oszkó, A., Sipos, P., and Dombi, A. The effect of particle shape on the activity of nanocrystalline TiO_2 photocatalysts in phenol decomposition. Part 3: The importance of surface quality. *Applied Catalysis B: Environmental*, 96(3-4):577-585, 2010.

[47] Orrego, S., Cortés, J., Amoresi, R., Simões, A., and Ramírez, M. Photoluminescence behaviour on Sr^{2+} modified $CaCu_3Ti_4O_{12}$ based ceramics. *Ceramics International*, 44(9):10781-10789, 2018.

[48] Mishra, P. and Kumar, P. Structural, dielectric and optical properties of [(BZT–BCT)-(epoxy-CCTO)] composites. *Ceramics International*, 41(2):2727-2734, 2015.

[49] Moura, F., Simoes, A., Deus, R., Silva, M., Varela, J. A., and Longo, E. Intense photoluminescence emission at room temperature in calcium copper titanate powders. *Ceramics International*, 39(4):3499-3506, 2013.

[50] Sedghi, R. and Heidari, F. A novel & effective visible light-driven TiO_2/magnetic porous graphene oxide nanocomposite for the degradation of dye pollutants. *RSC Advances*, 6(55):49459-49468, 2016.

[51] Ahmadipour, M., Arjmand, M., Ahmad, Z. A., and Pung, S. Y. Photocatalytic degradation of organic dye by sol–gel-synthesized $CaCu_3Ti_4O_{12}$ powder. *Journal of Materials Engineering and Performance*, 29:2006-2014, 2020.